Instituto de Engenharia
Mecânica e Gestão Industrial

PIBRAC-WP320
Initial results of FEA study

Pedro Portela, Pedro Bandeira, J. F. Silva Gomes

October 2005

1 Introduction and Scope

The purpose of this document is to report on the results of the Finite Elements analysis performed on the high power-PIBRAC piezoelectric motor.

2 Geometry, material properties and assumptions

This chapter will address the data used to develop the FE model. This includes the geometric data, provided by SAGEM, the mechanical and piezoelectric material properties and some assumptions regarding the behavior and operating conditions of the piezoelectric motor.

2.1 Geometry

The fundamental geometric characteristics and dimensions of the piezoelectric motor were taken from **version 7 (seven)** of the design spreadsheet. This development of this spreadsheet is of the responsibility of SAGEM. A summary of the geometric design parameters is liste in table 2.1. The significance of these parameters can be verified in figure 2.1 where a $\frac{1}{8}$ sector of the motor stator is represented. For convenience, the motor exterior and interior diameter are also represented.

Parameter name	Parameter symbol	Value
Leave mean radius	r_m	36.36
Leave delta radius	$\triangle r_m$	9.09
Leave exterior radius	r_e	40.91
Leave interior radius	r_i	31.82
Tangential ceramic thickness	e_c	2.54
Exterior leave thickness	e_m	5.07
Tangential ceramic width	$\triangle r_c$	8.82
Leave length	l_m	7.4
Tangential ceramic length	l_c	18.16
Rigid layer thickness	e_i	1.03
Elastic layer thickness	e_e	0.87

Table 2.1: Geometric data compiled from the design model (Modèle 7 spreadsheet.)

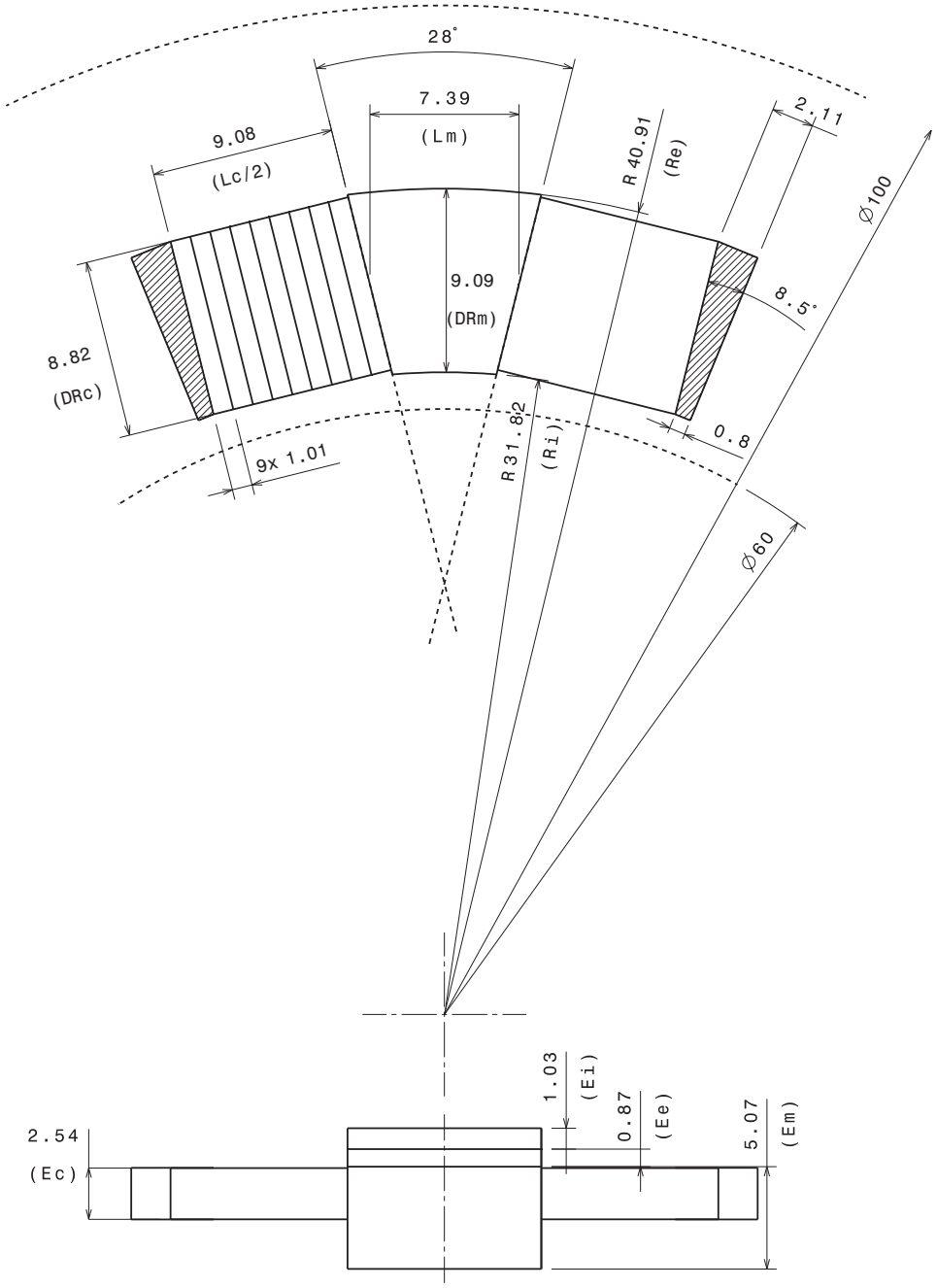

Figure 2.1: Technical drawing of the sector used in the analysis.

2.2 Material properties

In figure 2.2 the five different material assignments are shown. The wedges, the metallic block and the rigid layer are made of an isotropic steel. The elastic layer is made of a yet undefined material but must have a tangential stiffness of $K_t = 8.787N/m$.

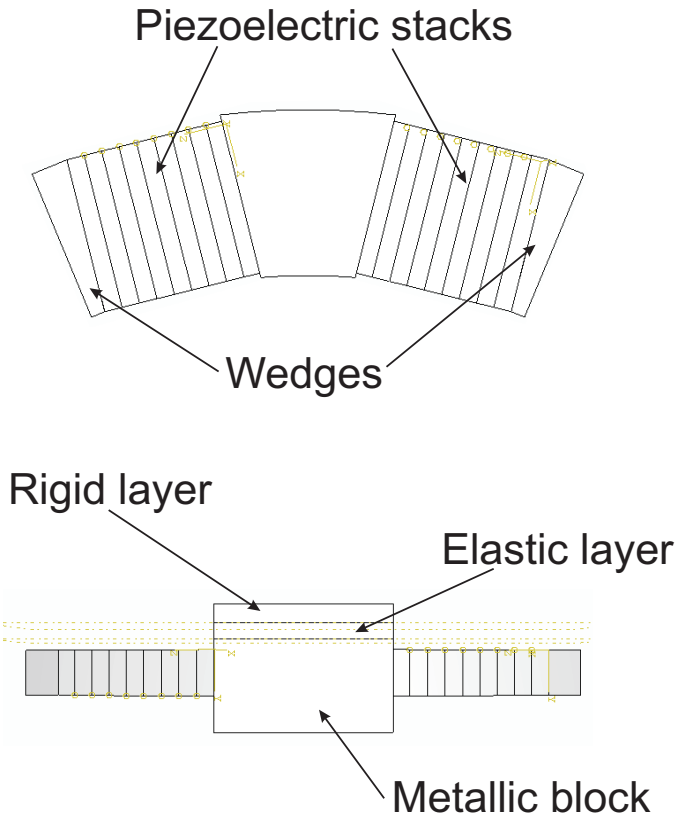

Figure 2.2: Illustration of the five different material assignments.

The mechanical properties of these materials are listed in table 2.2. The properties of the piezoceramic materials are listed separately in the following pages.

Material name	Young Modulus	Poisson ratio	Density
Metallic block	2.1E011	0.3	7700
Wedges	2.1E11	0.3	7700
Rigid layer	2E11	0.3	7850
Elastic layer	2.48E9	0.2	785

Table 2.2: Mechanical properties of the isotropic materials used in the model.)

The was determined by acknowledging that the tangential stiffness K_t can be given by

$$K_t = \frac{GA}{e_e} \tag{2.1}$$

where

G : is the shear modulus of the material

A : is the surface area of the elastic layer

e_e : is the thickness of the elastic layer

Additionally, the elastic layer's density is estimated to be roughly 2% of the density of steel. The piezoceramic mechanical properties can be considered orthotropic.

$$E = \begin{bmatrix} 7.69E10 \\ 7.69E10 \\ 5.09E3 \end{bmatrix} \text{ Pa}$$

The coordinate system associated to the piezoelectic elements is shown in figure 2.3.

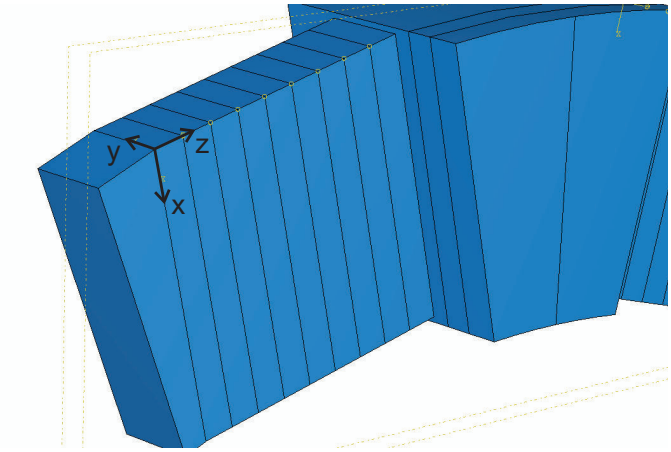

Figure 2.3: Material coordinate system for the piezoelectric elements.

The shear modulus is $G = 1.7E10$ and the density is $\rho = 7700kg/m^3V$. The dielectric matrix is given by

$$D = \begin{bmatrix} 7.04E-9 & 0 & 0 \\ 0 & 7.04E-9 & 0 \\ 0 & 0 & 5.95e-9 \end{bmatrix} \text{ F/m}$$

The electric field will be applied in the polling direction (z). Thus, the piezoelectric coefficient matrix as required by ABAQUS is mostly zero, except for three terms that correspond to the

effect produced by an electric field applied in the z or 3 direction. The piezoelectric stress coefficients are given by

$$e_3 = \begin{bmatrix} 9.86 & 0 & 0 \\ 0 & -2.8 & 0 \\ 0 & 0 & 14.7 \end{bmatrix} C/m^2$$

2.3 Loads and boundary conditions

For the eigenvalue extraction step, no loads were applied to the model, but two different sets of boundary conditions were applied. The first set, considers that the cyclic symmetry planes are clamped. This means that all the displacement components of every node on this surface are matched by an equal and opposite displacement on the surface adjacent to it. Alternatively, the displacement DOF's on these surfaces can be matched by a constraint equation that represents cyclic symmetry. The displacements of one surface (the slave surface) are equal to the displacements of the master surface. This is the most realistic boundary condition and so it was also used in parallel to the clamped boundary condition. The results are discussed in the next chapter.

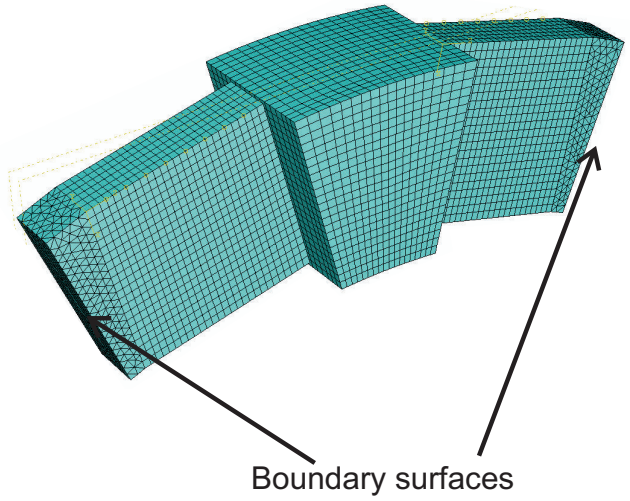

Figure 2.4: FE model mesh and boundary surfaces.

3 Analysis results and discussion

3.1 Eigenvalue analysis

Eigenvalue analysis was performed to verify the mode shapes and eigenfrequency of the piezoelectric motor both in the tangential and longitudinal or normal direction. The PIBRAC piezoelectric motor must have a tangential and normal mode of vibration at the same frequency of $35kHz$.

3.1.1 Tangential mode

Figure 3.1 represents the tangential eigenmode of the sector subjected to clamped boundary conditions.

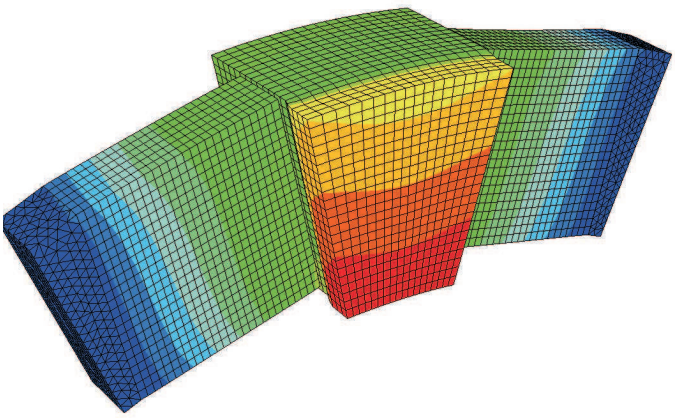

Figure 3.1: Tangential eigenmode with Clamped boundary surfaces. Frequency 34.810 kHz

Figure 3.2 represents the tangential eigenmode of the sector subjected to cyclic symmetry conditions. The cyclic symmetry mode for this eigenmode is four. This suggests that this is a local mode in four or the eight sector of the stator. This is coherent with the motor's operation.

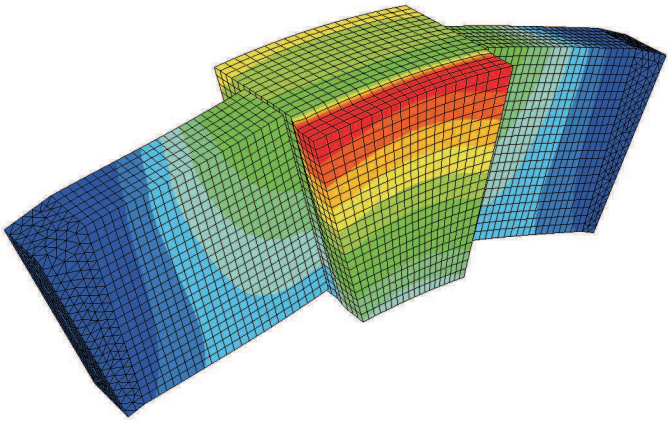

Figure 3.2: Tangential eigenmode with cyclic symmetric boundary conditions. Frequency 36.079 kHz.

The displacement fields for both cases are very similar. However there is a slight difference of $1.269kHz$ (3.6%) between both models that is explained by the difference in stiffness caused by the boundary conditions.

3.1.2 Normal mode

To determine the normal mode of vibration, the rotor and an additional stator was added to the assembly. The additional stator has an interface to the normal piezoelectric stack actuator that is responsible for the excitation of the longitudinal or normal mode. The material used for the rotor model was steel and cyclic symmetry boundary conditions were used on the side surfaces. Because the stator is free to rotate around the motor axis, the corresponding degree of freedom was released on this interface surface. All the others were restrained. Although the geometry used for the model is currently out-of-date the results of this first analysis is shown in figure 3.3.

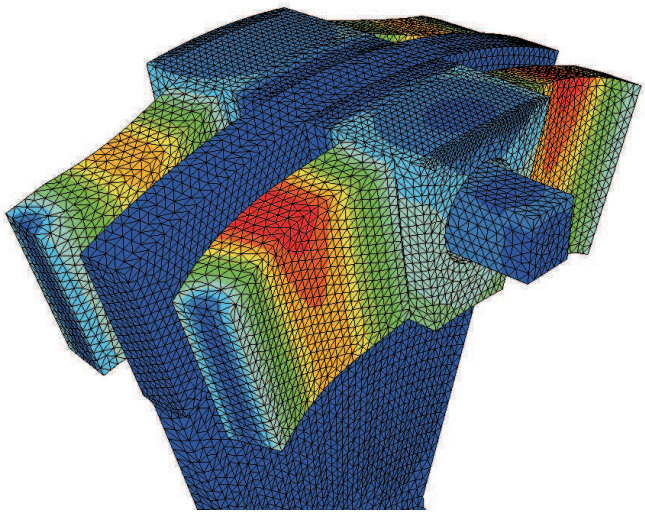

Figure 3.3: Normal eigenmode with cyclic symmetric boundary conditions. Frequency 29.360 kHz.

Attached to the opposite surface of the assembly is a mechanical spring with a spring constant of $K_s = 1.63e9N/m$.

3.2 Active piezoelectric analysis

The harmonic response of the tangential actuators was studied. A sinusoidal electric potential field was applied to the surfaces of the electrodes as shown in figure

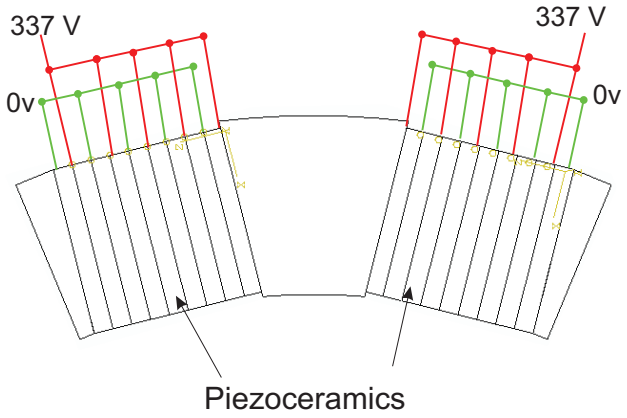

Figure 3.4: Activation voltage and electrodes

The electric field strength across one piezoceramic element is $E = \Delta V/t \Leftrightarrow \frac{337}{1.03E-3} = 334kV/m$, where t is the element's thickness, in this case 1.03 mm.l

3.2.1 Tangential mode

An additional damping property is needed in order to perform an accurate dynamic analysis. Abaqus allows the user to use several different damping models depending on the analysis types. The one used here was the steady state dynamics with direct integration. This is the only type that allows the use of a varying electric potential boundary condition. The damping model assumed with this procedure is the Rayleigh Damping model. Unlike the mode based steady state dynamics, the direct integration method does not depend of a previous frequency step (except to determine the frequency range and points). Direct integration methods use complex damping and assume a complex solution for the harmonic response. Rayleigh damping is a combination of two damping factors: a mass proportional damping and a stiffness proportional damping. For a given mode i the fraction of critical damping ξ_1 can be expressed in terms of the mass damping and stiffness damping factors respectively α_r and β_r

$$\xi_i = \frac{\alpha_r}{2\omega_i} + \frac{\beta_r \omega_i}{2} \tag{3.1}$$

The parameters are dependent on the material but were considered to be the same for all of the materials in the model. The analysis was performed in a very tight frequency range that includes only the eigenfrequency of interest, $34kHz$ to $35.5kHz$. The results that were registered were: peak tangential displacement of a point in the center of the rigid layer, quality factor and model damping. The peak tangential displacement, U_{max}, can be approximated by the linear displacement in the tangential direction given that the amplitudes are very small. Figure 3.5 represents the variation of the peak displacement versus stiffness proportional damping.

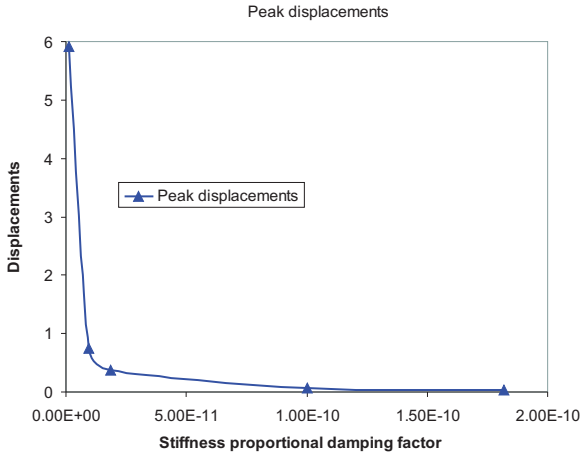

Figure 3.5: Peak displacements versus stiffness proportional damping factor

Figure 3.6 shows the variation of the mechanical quality factor versus the stiffness proportional damping.

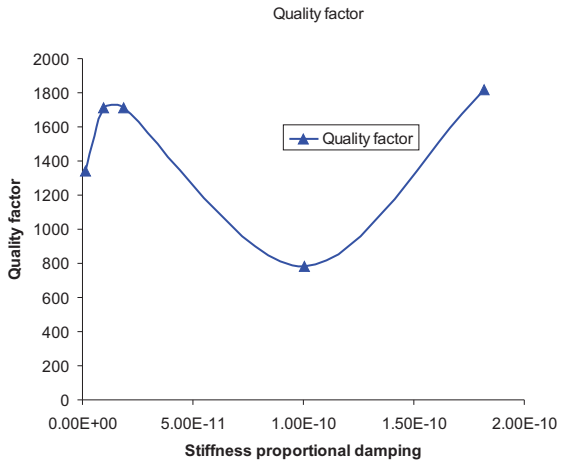

Figure 3.6: Quality factor versus stiffness proportional damping factor

The quality factor was determined from the displacement response curve and by using the relation

$$Q = \frac{1}{2\xi} = \frac{\omega_r}{\omega_2 - \omega_1} \tag{3.2}$$

where ω_2 and ω_1 are the half-power frequency points. Because ABAQUS does not provide analysis information on those spe-

cific points, it is necessary to linearly interpolate between the resonant frequency point and the ones adjacent to it.

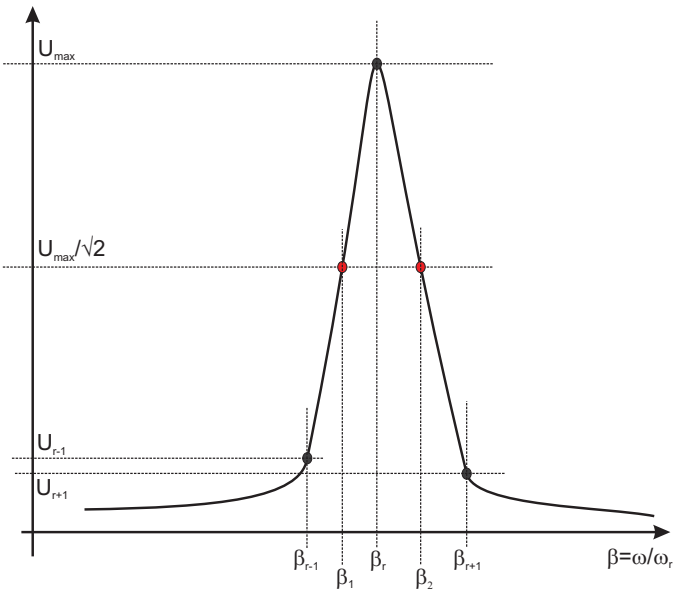

Figure 3.7: Displacement response curve

Again, using equation 3.2, it is possible to determine the fraction of critical damping of the model. A summary of the numerical results is listed in table 3.1.

Stiffness damping (s)	Displacement (μm)	Quality factor	ξ
1.82E-10	0.0383	1817	0.025%
1.0E-10	0.069	784	0.064%
1.88E-11	0.37	1710	0.029%
1.18E-12	5.9	1339	0.037%

Table 3.1: Dynamic analysis results summary.

The distribution of the electrical potential field and the Von Mises stress distribution is shown is figure 3.8 and figure 3.9.

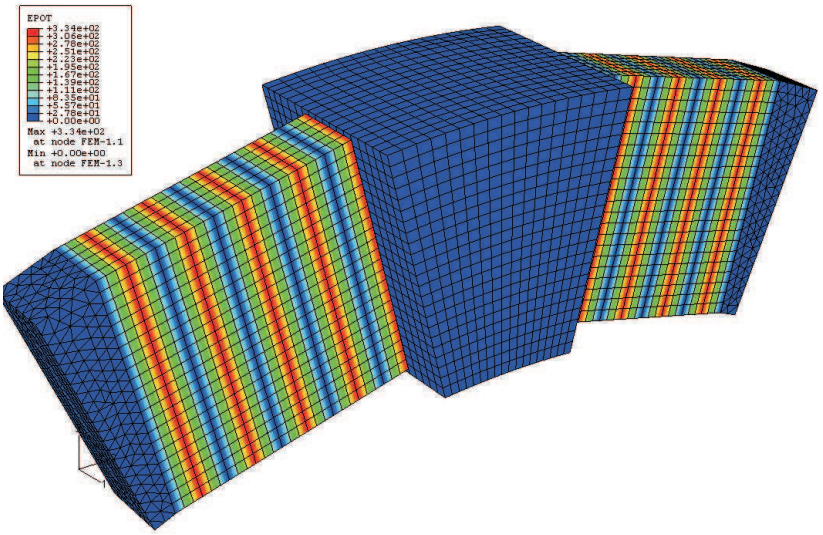

Figure 3.8: Applied electric potential field

As expected the potential difference varies between zero and 334 Volts. The peak value of the Von Mises equivalent stress is 65 MPa.

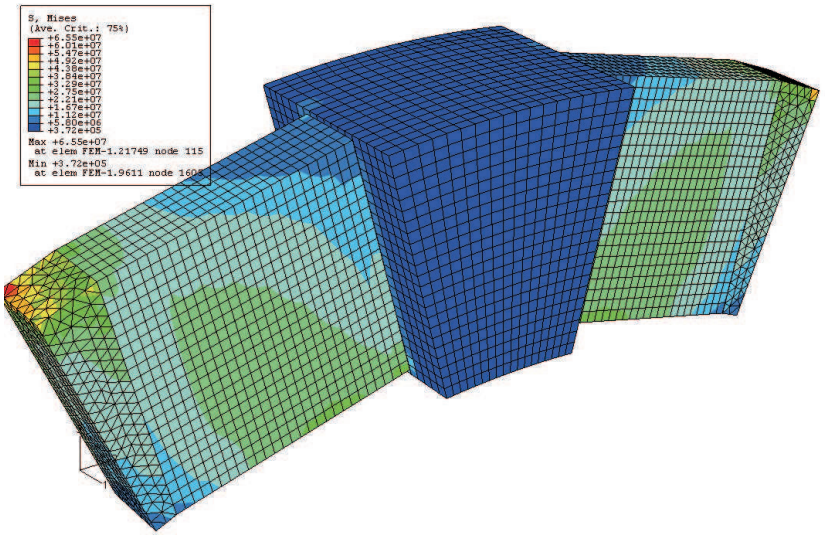

Figure 3.9: VonMises stress field

3.3 Preliminary conclusions and action items

1. The tangential eigenmode is well determined and satisfactory
2. The longitudinal mode value is close to the required (35 kHz) but still not close enough. The geometry needs to

be updated. The shape appears to be correct as it has a pinching movement of the rotor.

3. The harmonic analysis of the tangential movement shows a discrepancy with SAGEM's data. SAGEM reported a peak displacement of 6.06 μm and a quality factor of 50. The results in table 3.1 show that to achieve this displacement a quality factor of 1339 is needed which corresponds to a critical damping factor of 0.037%

4. Active analysis of the longitudinal mode must be done and coupled with the tangential one.